Real-time UV and column ozone from multi-channel UV radiometers deployed in the National Science Foundation's UV monitoring network

Germar Bernhard*, Charles R. Booth**, James C. Ehramjian***
Biospherical Instruments Inc., San Diego

ABSTRACT

Multi-channel moderate-bandwidth GUV filter radiometers have recently been added to the suite of instruments deployed in the US National Science Foundation Office of Polar Programs' UV monitoring network. The GUV instruments complement the stations' SUV-100 high-resolution scanning spectroradiometers, which have been monitoring UV levels in Antarctica, South America, and Alaska for more than a decade. The GUV instruments are used to help quality control SUV measurements, and to calculate total column ozone and a variety of biologically relevant UV integrals and dose-rates in real time. The results are updated every minute on web pages, and can be accessed via the website www.biospherical.com/nsf, or the stations' intranets. Online data may guide researchers on station in planning experiments, or for "first-look" analysis. The instruments underwent a detailed characterization. Their spectral response functions were measured with an apparatus that was specifically designed for this purpose. The apparatus and the data analysis method are described in detail with special attention given to a deconvolution method to correct measured data for the finite spectral resolution of the apparatus. The impact of uncertainties in measuring the spectral response of GUV channels on solar measurements is discussed. The GUV instruments are calibrated by comparison with a SUV-150B spectroradiometer, and dose-rates for 15 different biological action spectra are calculated based on an algorithm suggested by Dahlback[1]. A comparison of calibrated GUV and SUV data indicates that erythemal (CIE) irradiance can be derived from GUV measurements to within 3% relative to the SUV up to a solar zenith angle (SZA) of 80º. A similar level of agreement can also be reached for other action spectra. Ozone values derived from GUV measurements at San Diego agree to within 3 Dobson Units (DU) with SUV ozone data and within a few DU with Earth Probe TOMS satellite observations.

Keywords: Solar ultraviolet radiation, Antarctica, filter instruments, QA/QC

1. INSTRUMENTS

Real-time UV and ozone data are derived from measurements of multi-channel moderate-bandwidth GUV filter radiometers, designed and manufactured by Biospherical Instruments Inc. The instruments provide measurements in four approximately 10 nm wide UV bands centered at 305, 320, 340, and 380 nm. A fifth channel measures Photosynthetically Active Radiation (PAR) and is sensitive to visible radiation between 400 and 700 nm. The angular response of the radiometer's collector has virtually no azimuth dependence and its cosine error is smaller than ±3% (±7.5%) for zenith angles less than 65º (82º). The instrument and its data have been described in several publications[1-7].

GUV measurements were compared with measurements of a high-resolution SUV-150B spectroradiometer. The instrument is an advanced version of a SUV-150 spectroradiometer described previously[8,9]. Compared to its predecessor, the SUV-150B features an upgraded wavelength drive with optical encoders, which reduce wavelength uncertainties to ±0.015 nm. Furthermore, the instrument's collector is now connected with a quartz fiber bundle to the remainder of the instrument, which facilitates deployment in cold climates. The collector's cosine error is smaller than ±2% for zenith angles less than 75º. The instrument has a bandwidth of 0.67 nm. For solar measurements, it scans from 280 to 600 nm in steps of 0.2 nm.

* bernhard@biospherical.com; phone 1 619 686-1888; fax 1 619 686-1887; http://www.biospherical.com; Biospherical Instruments Inc., 5340 Riley Street, San Diego, CA 92110-2621, USA; ** booth@biospherical.com; *** jime@biospherical.com

2. SPECTRAL RESPONSE CHARACTERIZATION

The spectral response of GUV channels was measured with a tunable radiation source consisting of a 1000-Watt xenon arc lamp from Oriel Instruments and a grating double monochromator with prism predisperser designed and built by Biospherical Instruments Inc. The two single monochromators that make up the double monochromator are stacked on top each other and share a common shaft to which the gratings are mounted. The shaft holds a total of six gratings (three for each single monochromator) with different groove-spacing for different wavelength ranges, and is driven by a single stepper motor. This design warrants that the two single monochromators are always synchronized. For the characterization of GUVs, only two sets of gratings were used, namely gratings with 2400 and 1200 grooves per mm (g/mm).

The intensity of radiation leaving the exit of the monochromator is characterized with a silicon photodiode as a function of the monochromator's wavelength setting. For determining the wavelength mapping of the monochromator, the xenon lamp is replaced by a mercury discharge lamp. Table 1 gives an overview of the instrument's specifications.

Table 1: Specifications of apparatus for spectral characterization

Monochromator		
	Type	Czerny-Turner double monochromator in additive configuration with prism predisperser, designed and built by Biospherical Instruments Inc.
	Focal length	500 mm
	Focal ratio	f/5
	Dispersion	0.35 nm/mm with 2400 g/mm gratings; 0.69 nm/mm with 1200 g/mm gratings
	Bandwidth (FWHM)	1.35 nm with 2400 g/mm gratings; 2.6 nm with 1200 g/mm gratings
	Wavelength accuracy	±0.1 nm
Light source		1000-Watt xenon arc lamp from Oriel Instruments
Reference detector		Silicon photodiode, Newport Corporation, Model 818-UV, responsivity calibration traceable to NIST

The spectral response characterization of a GUV includes the following scans:

- Measurement of the spectrum of the mercury lamp with the silicon photodiode
- Measurement of the spectrum of the xenon lamp with the silicon photodiode
- Measurement of the GUV signals for each channel as a function of wavelength using the xenon lamp as light source
- Repetition of the mercury lamp measurement

From the two scans of the mercury lamp bracketing the GUV scan we determined that GUV response functions can be measured with a wavelength accuracy of better than ±0.1 nm. For the characterization of the GUV channels centered at 305, 320, 340, and 380 nm only measurements with the 2400 g/mm gratings are required. We also measured these channels with the 1200 g/mm gratings in order to analyze the effect of the monochromator's finite bandwidth on the retrieved response functions, and to explore the feasibility of deconvolution techniques to improve the accuracy of the characterization further (see below). The 2400 g/mm gratings can only be used up to 600 nm. For the characterization of the PAR channel, the 1200 g/mm gratings were utilized.

Data reduction includes the following steps:

- Wavelength correction of spectra measured with the silicon photodiode and each of the GUV channels,
- Subtraction of dark currents from the signals measured by the silicon photodiode and all GUV channels,
- Radiometric calibration of the net-signals of all GUV channels based on the scan with the silicon photodiode,
- Deconvolution of the calibrated GUV signals to reduce the effect of the monochromator's finite resolution,
- Normalization of the deconvolved result.

The deconvolution algorithm is based on the approximation:

$$\frac{R_D(\lambda)}{R_M(\lambda)} \approx \frac{R_M(\lambda)}{R_C(\lambda)}, \tag{1}$$

where $R_D(\lambda)$ is the deconvolved spectral response (which ideally is the true spectral response),
$R_M(\lambda)$ is the measured spectral response normalized to 1 at the maximum value, and
$R_C(\lambda)$ is the measured spectral response convolved with the slit function of the monochromator.

From $R_M(\lambda)$, $R_C(\lambda)$ can readily be calculated, allowing to estimate $R_D(\lambda)$ by rearranging Eq. (1). The deconvolved spectral response is somewhat affected by noise in the measurement. In order to reduce this effect, $R_M(\lambda)$ is set to 0.0001 if the normalized response is smaller than 0.0001. The deconvolved result is limited to four orders of magnitude due to this restriction.

Figure 1 illustrates the deconvolution technique with measurements of the 320 nm channel of GUV S/N 29236. The measurement was performed with the 2400 g/mm gratings of the test apparatus (bandwidth = 1.35 nm). To make the difference of the original and deconvolved response more apparent, only the cut-off at the long-wavelength side of the channel (i.e. λ > 321 nm) is shown. The measured spectral response $R_M(\lambda)$ is illustrated by the thin line. The deconvolved spectral response $R_D(\lambda)$ is represented by the thick line, which indicates that the true spectral response has a steeper cut-off than the original measurement.

The quality of the deconvolution technique can be checked by convolving $R_D(\lambda)$ with the slit function of the monochromator, and comparing the resulting function, denoted $R_{DC}(\lambda)$, with the original measurement $R_M(\lambda)$. If the deconvolution were perfect, $R_{DC}(\lambda)$ and $R_M(\lambda)$ would be equal. For the example shown in Figure 1, $R_{DC}(\lambda)$ and $R_M(\lambda)$ are barely distinguishable, suggesting that the accuracy of measurement of the test apparatus can indeed be improved by deconvolution. A similar analysis based on measurements with the 1200 g/mm gratings showed a less satisfactory agreement. When using this set of gratings, the bandwidth of the test apparatus is 2.6 nm. The smoothing introduced by the wider slit function appears to be too large to be accurately corrected by deconvolution.

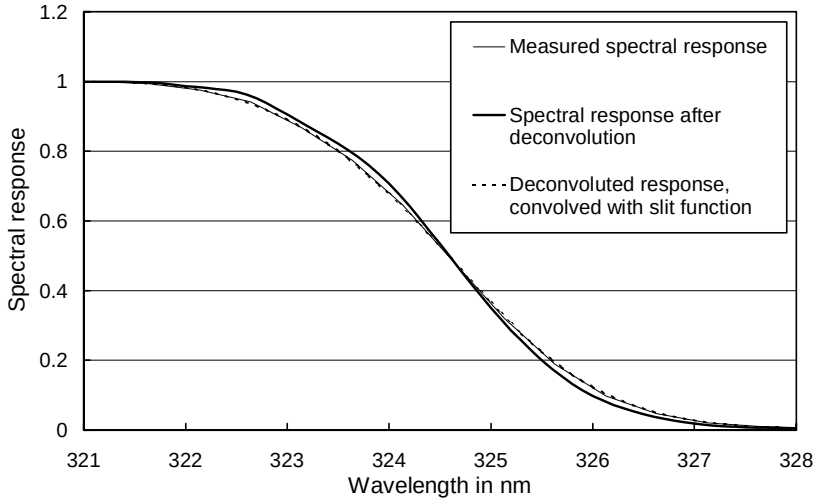

Figure 1: Comparison of measured (thin line) and deconvolved (thick line) spectral response of the 320 nm channel of GUV S/N 29236. The data set indicated by the broken line was calculated by convolving the deconvolved response $R_D(\lambda)$ with the slit function of the of the test apparatus.

Figure 2 shows the spectral response functions $R_D(\lambda)$ of the 305, 320, 340, and 380 nm channels for two GUV radiometers (serial numbers 9298 and 29236). There are several points that are worth mentioning:

- The short-wavelength limits of the 305 channel of both radiometers are shifted by approximately 8 nm against each other owing to the different set of filters used in both instruments. This has little impact on solar measurements as solar radiation below 290 nm is not penetrating the Earth's atmosphere. Almost all contribution to the GUV signal of the 305 nm channel stems from photons with wavelengths between 300 and 310 nm, where the response functions of the two instrument are very similar.
- The detector of the 305 nm channel is a phototube. The long-wave cut-off of the 305 nm channels is determined by the sensitivity of the phototube rather than the characteristics of the channel's interference filters. As the phototube has no significant sensitivity above 315 nm, photons with wavelengths in the UV-A or visible, which may reach the surface of the tube due to possible light leaks of the filters, are not detected.
- The responsivities of the 320, 340, and 380 nm channels are similar for both instruments but are shifted by 0.6-0.9 nm against each other. These shifts are caused by the different transmission characteristics of the interference filters used in the two instruments. Variations in the position of the center wavelength of the filters by several tenth of a nm are within the specifications of the filter manufacturer. Constraining this specification to smaller variations is cost prohibitive. It is therefore necessary to characterize the response functions of each filter radiometer individually to obtain the most accurate solar measurements.
- The right panel of Figure 2 indicates that the 320 nm channels of GUV S/N 9298 is also sensitive to radiation in the 330-380 nm band. Such light leaks may introduce significant errors in solar measurements, particularly when a UV-B detector is also sensitive to radiation in the visible. A comparison of simultaneous solar irradiance measurements with GUV S/N 9298 and the SUV-150B spectroradiometer indicated that the leakage problem is too small to affect solar data appreciably.

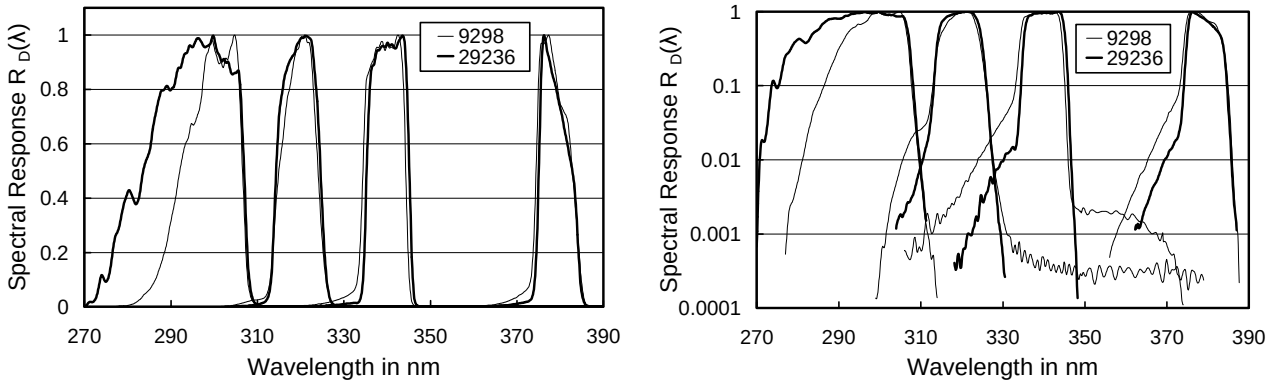

Figure 2: Spectral response functions $R_D(\lambda)$ of the 305, 320, 340, and 380 nm channels of two GUV radiometers (S/N 9298 and 29236) in linear (left panel) and logarithmic (right panel) presentation.

3. CALIBRATION

The calibration factors k_i for each GUV channel i were determined with a method first proposed by Dahlback[1]:

$$k_i = \frac{V_i - O_i}{\int_0^\infty R_{D_i}(\lambda)\ E(\lambda)\ d\lambda} = \frac{V_i - O_i}{W_i}, \qquad (2)$$

where $E(\lambda)$ is spectral irradiance at the place of the GUV's collector,

V_i is the signal of channel *i*,

O_i is the offset of channel *i* typically inferred from measurements at night,

$R_{D_i}(\lambda)$ is the deconvolved, normalized spectral response of channel *i*, and

W_i is spectral irradiance weighted with the spectral response of channel *i*.

The values of k_i are independent of the light source that produces $E(\lambda)$, if $R_{D_i}(\lambda)$ represents the true spectral response functions of the radiometer. In this study, $E(\lambda)$ stems either from standard lamps, which have calibrations traceable to the National Institute of Standards and Technology (NIST), or the Sun. In the latter case, the solar spectral irradiance was measured by the SUV-150B, which was taking scans side-by-side with the GUV to be calibrated.

Figure 3 shows a comparison of solar measurements from the 305 nm channel of GUV S/N 9298 and the SUV-150B. Prior to this comparison, the calibration factor k_{305} of the GUV was calculated by regressing the net-signal of the GUV (numerator of Eq. (2)) against the GUV-response-weighted spectral irradiance from the SUV-150B (denominator of Eq. (2)). Accurate synchronization of both instruments is critical for this correlation. The GUV minute-by-minute measurements were interpolated to the time when the SUV-150B was scanning at 305 nm. Owing to the way k_{305} is established, a good agreement of GUV and SUV data at small SZAs can be expected. Figure 3 demonstrates that a high level of agreement is also achieved at SZAs as large as 85º: with the exception of three points, the ratio of GUV and SUV-150B measurements agrees to within ±5% and the relative standard deviation is 2.2%. The three outliers occur at SZAs larger than 82º when irradiance levels are more than three orders of magnitude below the noon-time maximum (Figure 3D).

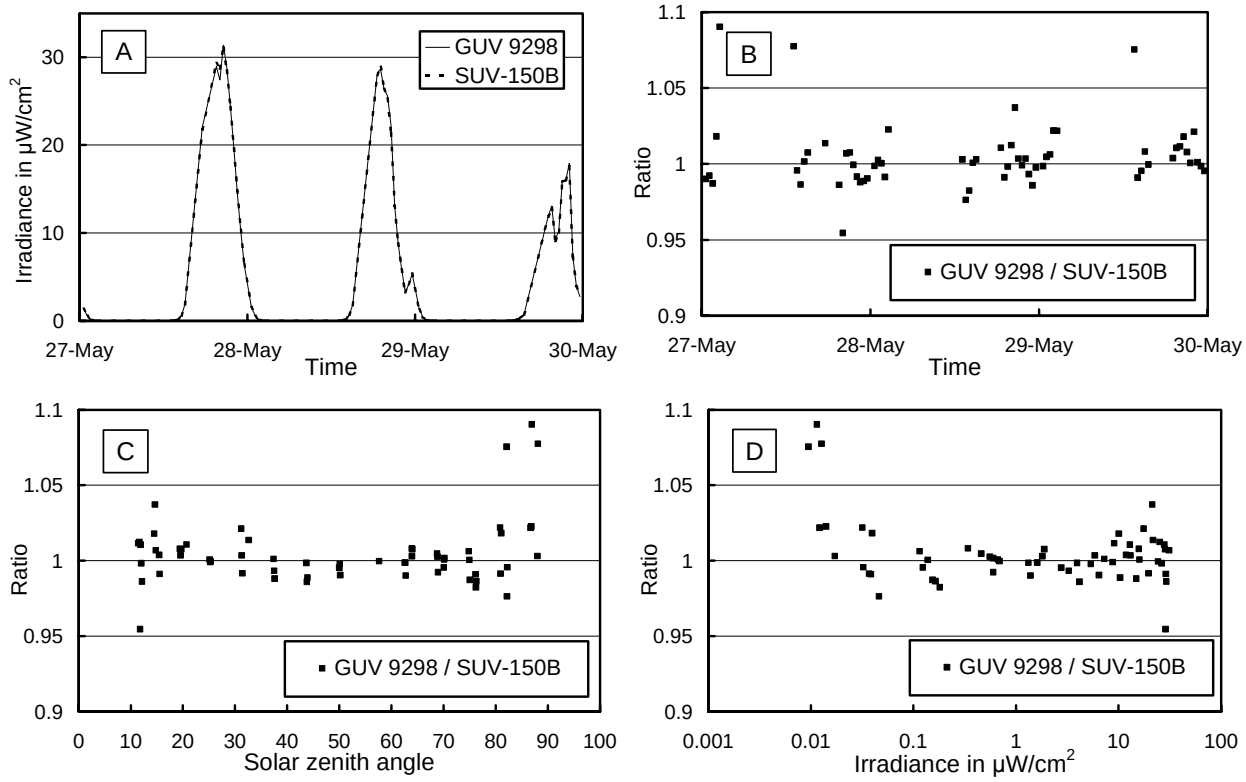

Figure 3: Comparison of measurements from the 305 nm channel of GUV S/N 9298 and the SUV-150B. The calibration factor k_{305} of the GUV was calculated by regressing GUV measurements against the weighted SUV-150B spectra. Panel A: Irradiance measured by GUV and SUV as a function of time. Panel B: Ratio GUV / SUV as a function of time. Panel C: Ratio GUV / SUV as a function of solar zenith angle. Panel D: Ratio GUV / SUV as a function of spectral irradiance (Note the logarithmic x-axis).

The high level of agreement of GUV and SUV-150B data could only be achieved since the spectral response functions of the GUV were accurately known. In order to demonstrate this, we deliberately shifted the measured response functions of GUV S/N 9298 by 0.5 nm, and repeated the analysis of Figure 3. A comparison of the shifted and unshifted data sets is presented in Figure 4. The effect of the shift is most pronounced for the 305 nm channel (Figure 4A) due to the rapid change of the solar spectrum in this wavelength range. At small SZA, the ratio GUV/SUV is close to unity also for the shifted data set due the way the calibration is established. At SZA=75°, both data sets disagree by 14%. The reason for this disagreement is due to the fact that the shape of the solar spectrum changes as a function of SZA over the 10-nm wide wavelength interval where the GUV 305 nm channel is sensitive. The relative change of the spectral distribution of solar radiation is sufficiently different for the shifted and unshifted wavelength intervals to explain the SZA dependence indicated in Figure 4A. The change of the solar spectrum with SZA is much smaller at 320 nm, resulting in a smaller (but still significant) difference of the shifted and unshifted datasets (Figure 4B).

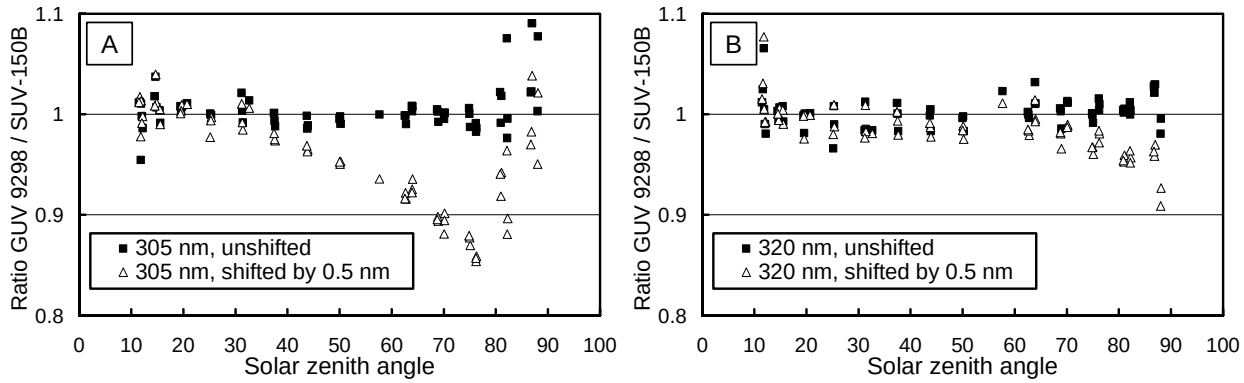

Figure 4: Comparison of measurements from the 305 and 320 nm channels of GUV S/N 9298 and the SUV-150B using either the measured, unshifted GUV response functions $R_{D_i}(\lambda)$ (solid squares), or response functions constructed by shifting $R_{D_i}(\lambda)$ by 0.5 nm (open triangles). Panel A: Comparison for the GUV 305 nm channel (the unshifted data set is identical with the one shown in Figure 3C). Panel B: Comparison for the GUV 320 nm channel.

A further validation of the accuracy of the calibration factors k_i can be obtained by evaluating the results of solar- and lamp-based calibrations. Figure 5 presents a comparison of calibration factors established with the two methods for three different GUVs (serial numbers 29235, 29236, and 9298). The spectral response functions of all instruments have been measured as described in Section 2. In addition, calibration factors for GUV S/N 9298 were compared that were calculated with the set of shifted response functions discussed above.

Figure 5 shows that solar- and lamp-based calibration factors agree to within ±3% if the measured response functions are used in Eq. (2). This is a good result as differences of less than 3% are well within the measurement uncertainties of the SUV-150B, and the uncertainty of the lamp-based GUV calibration. In contrast, if the shifted response function for the 305 nm channel of GUV S/N 9298 is used, solar- and lamp-based calibration factors deviate by 14%. By comparing the difference in the factors for the shifted and unshifted results, it was determined that solar data from the 305 nm channel will be incorrect by 12% if the calibration factor of this channel is established from a lamp measurement, and the response function used for the calculation has a wavelength error of 0.5 nm.

Figure 5 also indicates that wavelength shifts have a much smaller effect for the 320, 340, and 380 nm channels. For example, the effect of a shift of 0.5 nm on the 320 nm channel is only 1.1%. This suggests that accurate solar measurements can be expected from lamp-based calibrations for all but the 305 nm channel, even if the response functions used for the calibration are not well defined. However, differences between the actual response function and the function used for the calibration may exist that cannot be characterized by a shift of the center wavelength alone. For example, Figure 2 indicates that the differences between filters may be substantial, even if they belong to the same batch. In order to avoid calibration errors related to inaccurately known response functions, and to gain the most accurate solar data, we believe that a thorough characterization of all channels is advisable.

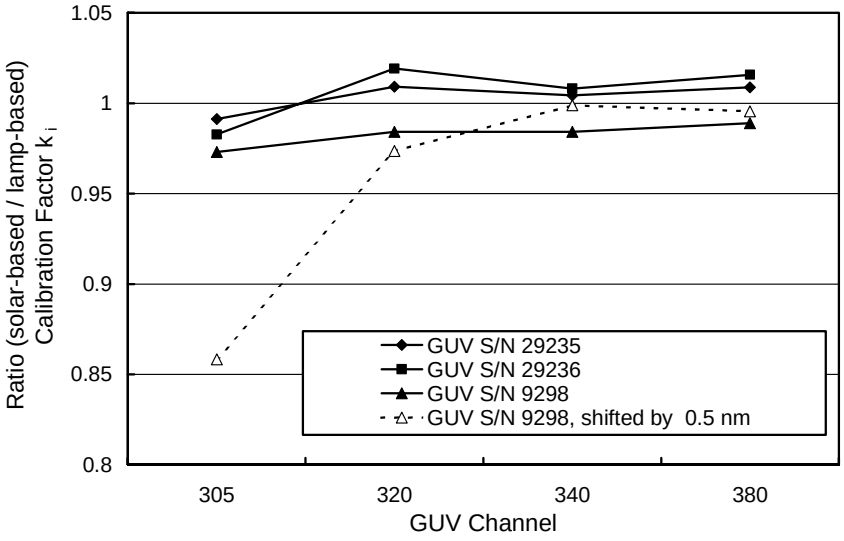

Figure 5: Comparison of solar- and lamp-based calibration factors k_i for three different GUV radiometers. The calibration factors marked with solid symbols were calculated with the measured response functions of the radiometers. The data set marked with open triangles was calculated with the shifted response functions of GUV S/N 9298 (shift = 0.5 nm) to investigate the effect of wavelength errors on the resulting calibration factors.

4. DATA PRODUCTS

The conversion from response-function-weighted irradiance W_i to useful data products *D*, such as erythemal irradiance, is performed with the method suggested by Dahlback[1] In brief, *D* is approximated by a linear combination of the net-voltages from the GUV channels:

$$D = \sum_i a_i (V_i - O_i) \tag{3}$$

The coefficients a_i are calculated by solving the system of linear equations (see also Eq. (7) of Dahlback[1]):

$$\sum_i \left(a_i k_i \int_0^\infty R_{D_i}(\lambda) \;\; E_{M_j}(\lambda) \;\; d\lambda \right) = \int_0^\infty A(\lambda) \;\; E_{M_j}(\lambda) \;\; d\lambda \,, \tag{4}$$

where $A(\lambda)$ is the action spectrum of the biological effect under consideration, and $E_{M_j}(\lambda)$ are model spectra calculated for different SZA and ozone columns. These spectra are required to quantify the relative spectral difference between the response functions and the action spectrum. For this study, model spectra were calculated with the radiative transfer model UVSPEC/libRadtran[10]. The values of a_i determined with this method are not very sensitive to the set of model spectra used. However for most accurate results, the model input parameters (e.g. ground albedo and altitude) should match the prevailing conditions at the deployment site of the GUV. The number of channels *i*, may range between 1 and 4, depending on the action spectrum used, and the number of model spectra required for the inversion has to match this number. For example, to calculate the set of coefficients a_i for the erythema action spectrum for a GUV deployed at San Diego, we used all GUV channels with the exception of the PAR channel, and four model spectra calculated for combinations of SZA and total ozone of 30º, 250DU; 30º, 400DU; 70º, 250DU; and 70º, 400DU.

Alternatively to the conversion method outlined above, the coefficients a_i could also been determined by a multi-linear regression of the GUV signals against biologically weighted SUV-150B spectra[2]. The inversion method has several advantages compared to this alternative method:

- The prevailing conditions at the location where the calibration is established may be different from the conditions at the deployment site. For example, if a GUV is calibrated with the alternative method in San Diego and deployed in Antarctica, prevailing SZA and total ozone and albedo conditions will be very different.
- A linear regression is most sensitive to the highest values, which is not the case for the inversion method.
- If the response functions $R_{D_i}(\lambda)$ are accurately known, the coefficients a_i can be calculated from lamp-based calibration factors k_i. It is therefore not required to operate a GUV side-by-side with a high-resolution spectroradiometer for several days, as in the case of the alternative method.

We are currently calculating 15 different wavelength integrals and 15 different dose-rates from GUV data with the method outlined above. Table 2 gives an overview of the wavelength bands and action spectra implemented.

Figure 6 shows a comparison of GUV and SUV-150B results for four data products, namely UV Index[11], DNA-damaging radiation[12], generalized plant response[13], and inhibition of photosynthesis in Antarctic phytoplankton[14]. The data is based on measurements at San Diego performed between May 27 and May 30, 2003. The GUV was calibrated by comparison with the SUV-150B, with the inversion algorithm described above. The afternoon of "Day 1" and morning of "Day 2" were cloudless, the remaining periods included scattered clouds and overcast skies. For the cloudless period, GUV and SUV measurements agree to within ±3% for all four effects. This is a good result considering the differences in the action spectra of the four effects: the UV Index has 90% contribution from the UV-B radiation; effects leading to DNA and "generalized" plant damage are even more weighted toward the UV-B. Inhibition of phytoplankton photosynthesis on the other hand has a large contribution from the UV-A. For cloudy periods, there is a larger scatter between GUV and SUV measurements, which is mostly due to the different sampling schemes of the two instruments: the GUV reports one-minute averages, whereas the SUV requires several minutes to scan between 290 and 400 nm during which radiation levels may change.

Figure 7 presents a comparison of total column ozone values calculated from the GUV and SUV-150B measurements. GUV ozone values were derived with a lookup-table, which relates total column ozone to SZA and the ratio of GUV measurements performed with the 305 and 340 nm channels. The retrieval method is similar to the method described by Stamnes et al.[15] SUV-150B ozone values were derived with an algorithm, which has recently been proposed.[16] The method compares the measured UV spectrum with a set of model spectra that were calculated for different ozone values[#]. Figure 7 demonstrates that GUV and SUV ozone values agree to within 3 DU, and measurements of both instruments agree to within 12 DU with Earth Probe TOMS observations. All days show a diurnal variation of about 15 DU, which could partly be real and partly be caused by aerosols influence. A discussion of this variation is beyond the scope of this paper.

5. WEB SITE IMPLEMENTATION

GUV raw-data are polled from the logging computers, and all data products listed in the Table 1 are calculated. The results are displayed on web pages, which are updated every minute, and accessible either via our website www.biospherical.com/nsf, or via the intranets of the Antarctic research stations. The web pages typically show graphs of the UV Index, Photosynthetically Active Radiation (PAR), and total ozone column, covering a period of two days. Other data products or periods can be selected by an easy-to-use user interface. Data in ASCII format is also available for download.

[#] Changing radiation levels during a scan of the SUV, which may be caused by changing cloud cover, will lead to scatter in the retrieved ozone values. For the period shown in Figure 7, the scatter was larger than typical as the SUV was measuring at a very slow rate, requiring 8.75 minutes to scan from 300 to 335 nm. The normal period required for this wavelength interval is 1.5 minutes. Ozone values were only included in Figure 7 if values derived from consecutive spectra deviated by less than 4%.

Table 2: GUV data products

Spectral irradiance:[a]
305 nm, 320 nm, 340 nm, 380 nm, 400 nm, 500 nm, and 600 nm

Integrals:[b]
290– 315 nm, 290–320 nm, 315–360 nm, 320–360 nm, 360–400 nm, 315–400 nm, 320–400nm, and 400–600 nm

Dose-rates:

Effect	References	Remarks
Erythema	*CIE*[11], *Komhyr and Machta*[17], *Diffey*[18], *Anders et al.*[19]	Four different action spectra are implemented.
UV Index	*CIE*[11]	
DNA damage	*Setlow*[12]	Four parameterizations of the action spectrum are implemented.
Skin cancer in mice	*Gruijl et al.*[20]	Often referred to as SCUP-m
Skin cancer in mice corrected for human skin	*Gruijl et al.*[20]	Often referred to as SCUP-h
Generalized plant resp.	*Caldwell*[13]	
Plant growth	*Flint and Caldwell*[21]	
Damage to anchovy	*Hunter et al.*[22]	
Inhibition of phytoplankton carbon fixation	*Boucher and* Prezelin [23]	
Inhibition of phytoplankton photosynthesis of phaeodactylum and prorocentrum	*Cullen et al.* [24]	
Inhibition of photosynthesis in Antarctic phytoplankton	*Neale and Kieber*[14]	

Additional:
Spectral irradiance weighted with the response of several broadband filter radiometers, Photosynthetically Active Radiation (PAR), total column ozone.

[a] The "action spectra for the calculation of spectral irradiances are triangular functions with a bandwidth of 1 nm FWHM centered at the specified wavelengths.

[b] The "action spectra" for the calculation of integrals are rectangular functions set to one within the specified interval and to zero outside this interval.

6. CONCLUSIONS AND OUTLOOK

If accurately characterized and calibrated, data from multi-channel filter radiometers can provide accurate measurements of biologically relevant UV levels and total column ozone. For achieving the highest level of accuracy, the instruments' response functions have to be characterized. As has been shown in Section 3, a 0.5 nm wavelength error in the response function may lead to errors of more than 10% in solar UV-B measurements. The calibration of filter radiometers can therefore be equally or even more demanding as the calibration of spectroradiometers. However, the retrieval and quality control of data products derived from filter instrument raw data is easier to achieve than for spectroradiometric measurements, which makes filter radiometers ideal for providing calibrated data in real-time. Furthermore, filter instruments are easier to deploy and maintain due to their simpler design, and offer data at a higher sampling rate. Although drifts in sensitivity over time have been reported[7] (e.g. 4% per annum), filter radiometers usually have a better short-term stability than spectroradiometers. This makes them useful for quality control of spectroradiometric measurements, which is the second reason why GUV instruments have recently been added to all sites of the NSF monitoring network. However, the instruments cannot replace the SUV-100 instruments deployed at those sites, as spectroradiometers have proven to be the most accurate instruments to monitor UV radiation at the Earth's surface [25] and additionally provide spectra at high-resolution, which are required for many applications in atmospheric research.

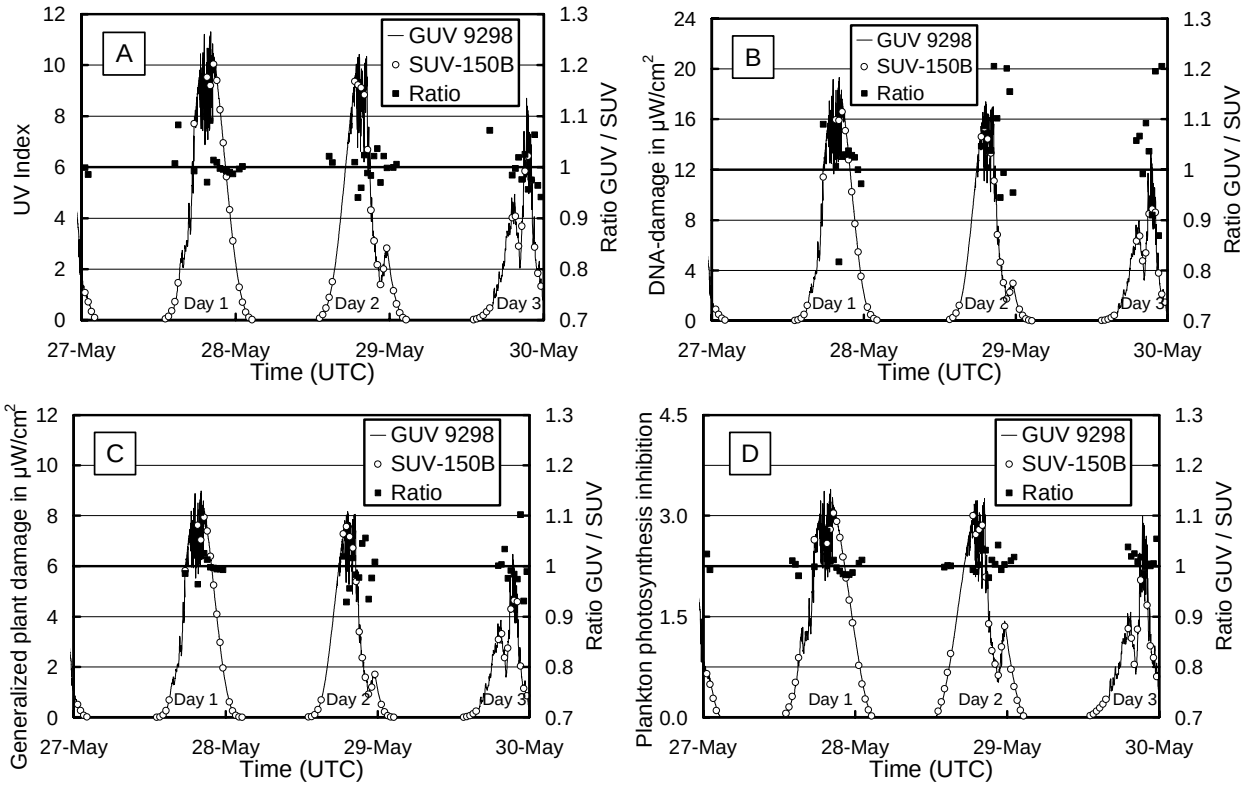

Figure 6: Comparison of four different data products measured by GUV S/N 9298 and SUV-150B at San Diego between May 27 and May 30, 2003. The ratios of GUV and SUV measurements are shown for periods when radiation levels exceed 10% of the maximum levels observed at noon. Panel A: UV Index; Panel B: DNA-damaging radiation, Panel C: Generalized plant response; Panel D: Inhibition of photosynthesis in Antarctic phytoplankton.

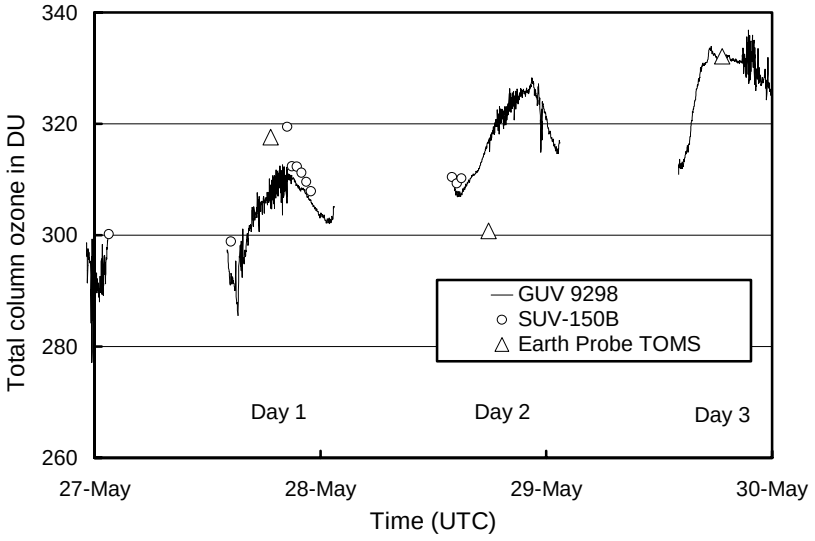

Figure 7: Comparison of total column ozone measured by GUV S/N 9298, SUV-150B and Earth Probe TOMS satellite at San Diego between May 27 and May 30, 2003.

ACKNOWLEDGMENTS

The NSF/OPP UV Monitoring Network is operated and maintained by Biospherical Instruments Inc. under a contract from the NSF Office of Polar Programs (Dr. Polly Penhale) via Raytheon Polar Services. The design and construction of the spectral test apparatus was overseen by David Goebel and implemented with help from Patrick White, Rick Reynolds, and James Robertson. The website implementation was programmed by Vi Quang.

REFERENCES

1. A. Dahlback, "Measurements of biologically effective UV doses, total ozone abundances, and cloud effects with multichannel, moderate bandwidth filter instruments", *Appl. Opt.*, **35**(33), 6514-6521, 1996.
2. C.R. Booth, T. Mestechkina, and J.H. Morrow, "Errors in the reporting of solar spectral irradiance using moderate bandwidth radiometers: an experimental investigation", in: *Ocean Optics XII*, SPIE, Vol 2258, 654-663, 1994.
3. C.R. Booth, "Synthetic UV spectroradiometry", in: *IRS'96 Current Problems in Atmospheric Radiation*, edited by W.L. Smith and K. Stamnes, Deepak Publ. Hampton, 849-852, 1997.
4. H.A. Fuenzalida, "Global ultraviolet spectra derived directly from observations with multi-channel radiometers", *Appl. Opt.*, **37**(33) 7912-7919, 1998.
5. T.M Thorseth and B. Kjeldstad, "All-weather ultraviolet solar spectra retrieved at a 0.5 Hz sampling rate", *Appl. Opt.*, **38**(30), 6247-6252, 1999.
6. T.M. Thorseth, B. Kjeldstad, B. Johnsen, "Comparison of solar UV measurements performed with spectroradiometer and moderate bandwidth multichannel radiometer for different cloud conditions", *J. Geophys. Res*., **105(**D4), 4809-4820, 2000.
7. B. Johnson, O. Mikkelborg, M. Hannevik, L.T. Nilsen, G. Saxebol, K.G. Blaasaas, *The Norwegian UV-monitoring program. Period 1995/96 to 2001*, Stralevern Rapport 2002:4 Osteras: Norwegian Radiation Protection Authority, 2002.
8. G. Bernhard, C.R. Booth, J.C. Ehramjian, and V.V. Quang, *NSF Polar Programs UV Spectroradiometer Network 2000-2001 Operations Report*, pp. 2-8 – 2-10, Biospherical Instruments Inc., San Diego, 2003.
9. K. Lantz, P. Disterhoft, E.A. Early, J. DeLuisi, A. Thompson, J. Berndt, L. Harrison, P. Kiedron, J. Ehramjian, G. Bernhard, L. Cabasug, J. Robertson, W. Mou, T. Taylor, J. Slusser, D. Bigelow, B. Durham, G. Janson, D. Hayes, M. Beaubien, and A. Beaubien, "The 1997 North American interagency intercomparison of ultraviolet spectroradiometers including narrowband filter radiometers", *J.Res.Natl.Inst.Stand.Technol*., **107**, 19-62, 2002.
10. B. Mayer, G. Seckmeyer, and A. Kylling, "Systematic longterm comparison of spectral UV measurements and UVSPEC modeling results", *J. Geophys. Res.*, **102**(D7), 8755-8768, 1997. The radiative transfer model UVSPEC/libRadtran is also available at www.libradtran.org.
11. A.F. McKinlay and B.L. Diffey, "A reference action spectrum for ultraviolet induced erythema in human skin", in: *Commission International de l'Éclairage (CIE), Research Note*, **6**(1), 17-22, 1987.
12. Setlow, R.B. "The wavelength in sunlight effective in producing skin cancer: a theoretical analysis", *Proceedings of the National Academy of Science, USA*, **71(**9), 3363-3366,1974.
13. M.M. Caldwell, "Solar UV irradiation and the growth and development of higher plants", in: *Photophysiology*, edited by A.C. Giese, Volume 6, Chapter 4, pp. 131 - 177, 1971.
14. P.J. Neale and D.J. Kieber, "Assessing biological and chemical effects of UV in the marine environment: Spectral weighting functions", in: *Issues in Environmental Science and Technology No. 14*, edited by R.E. Hester and R.M. Harrison, Royal Society of Chemistry, Cambridge, UK, 2000.
15. K. Stamnes, J. Slusser, and M. Bowen, "Derivation of total ozone abundance and cloud effects from spectral irradiance measurements", *Appl. Opt.*, **30**(30), 4418-4426, 1991.
16. G. Bernhard, C.R. Booth, and R. McPeters, "Calculation of Total Column Ozone from Global UV Spectra at High Latitudes", *J. Geophys. Res.*, 2003, in press.
17. W.D. Komhyr and L. Machta, "The relative response of erythema", in: *The Perturbed Troposphere of 1990 and 2020* , Vol. IV, CIAP, Dept. of Transportation, Washington. DC., 1973.
18. B.L. Diffey, "A comparison of dosimeters used for solar ultraviolet radiometry", *Photochem. Photobiol.*, **46**, 55-60, 1987.
19. A. Anders, H.-J. Altheide, M. Knaelmann, and H. Tronnier, "Action spectrum for erythema in humans investigated with dye lasers", *Photochemistry and Photobiology*, **61**(2), 200-205, 1995.

20. F.R. Gruijl, H.J.C.M. Sterenborg, P. D. Forbes, R.E. Davies, C. Cole, G. Kelfkens, H. van Weelden, H. Slaper, and J. C. van der Leun, "Wavelength dependence of skin cancer induction by ultraviolet irradiation of albino hairless mice", *Cancer Res*., **53**, 53-60, 1993.
21. S. D. Flint and M. M. Caldwell, "A biological spectral weighting function for ozone depletion research with higher plants", *Physiol. Plant.*, **117**,137–144, 2003.
22. J.H. Hunter, J.H. Taylor, and H.G. Moser, "The effect of ultraviolet irradiation on eggs and larvae of the northern anchovy, Engraulis mordax, and the pacific mackerel, Scomber Japonicus, uring the embryonic stage", *Photochem. and Photobiol.*, **29**, 325-338, 1979.
23. N.P Boucher, B.B. Prezelin, "An in situ biological weighting function for UV inhibition of phytoplankton carbon fixation in the Southern Ocean", *Marine ecology progress series*, **144**, 223-236, 1996.
24. J.J. Cullen, P.J. Neale, and M.P.Lesser, "Biological weighting function for the inhibition of phytoplankton photosynthesis by ultraviolet radiation", *Science*, **258**, 646-649, 1992.
25. G. Seckmeyer, A. Bais, G. Bernhard, M. Blumthaler, C.R. Booth, P. Disterhoft, P. Eriksen, R.L. McKenzie, M. Miyauchi, and C. Roy, "Instruments to measure solar ultraviolet radiation. Part 1: Spectral instruments", World Meteorological Organisation, Global Atmospheric Watch Publication No. 125, WMO TD No. 1066, Geneva, Switzerland, 2001.